Detection of a persistent meteoric metal layer in the Martian atmosphere

M. M. J. Crismani[1]*, N. M. Schneider[1], J. M. C. Plane[2], J. S. Evans[3], S. K. Jain[1], M. S. Chaffin[1], J. D. Carrillo-Sanchez[2], J. I. Deighan[1], R. V. Yelle[4], A. I. F. Stewart[1], W. McClintock[1], J. Clarke[5], G. M. Holsclaw[1], A. Stiepen[6], F. Montmessin[7] and B. M. Jakosky[1]

Interplanetary dust particles sporadically enter planetary atmospheres at orbital velocities and ablate as collisions occur with ambient gases to produce a persistent layer of metallic atoms (for example, Fe, Mg, Na) in their upper atmospheres. Such layers are well studied at Earth, but have not been directly detected elsewhere in the Solar System. Here we report the detection of a meteoric layer consisting of Mg^+ ions near an altitude of 90 km in the Martian atmosphere from ultraviolet remote sensing observations by NASA's MAVEN spacecraft. We observe temporal variability in the Mg^+ layer over the course of a Martian year, moving up and down in altitude seasonally and in response to dust storms, and displaying diurnal fluctuations in density. We also find that most meteor showers do not significantly perturb this layer, which constrains the fluence of eleven observed Martian meteor showers to less than our estimated global dust flux. The persistence and variability of the Mg^+ layer are difficult to explain with existing models and reconcile with other transient layers of ions observed in the Martian ionosphere. We suggest that the transient layers are not sourced from the persistent Mg^+ layer and thus not derived from meteoric material, but are ambient ions produced by some unknown mechanism.

High-speed collisions with air molecules cause rapid heating of interplanetary dust particles (IDPs), melting and evaporating their constituent minerals[1–3]. This ablation process deposits a variety of atomic constituents at the $\sim 1\,\mu bar$ level (80–110 km on Earth). Non-volatile elements such as Mg, Fe and Na act as direct tracers of the ablation process, as no other processes transport these species to these altitudes. These elements are in approximate equilibrium between supply through ablation[4] and loss by chemical reactions forming oxides, hydroxides and carbonates, which subsequently polymerize into particles called meteoric smoke[5]. Meteoric smoke particles most likely provide condensation nuclei for high-altitude CO_2 ice clouds at Mars[6]. In addition to the quasi-steady-state supply from random (or 'sporadic') meteors, the ablation of cometary dust during meteor showers can supply additional metals to the upper atmosphere.

The Mars Atmosphere and Volatile Evolution (MAVEN) mission was designed to study the response of Mars' upper atmosphere to solar influences[7], which also renders it capable of detecting the influence of IDPs. This capability was clearly demonstrated during the exceptionally close pass of comet C/2013 A1 (Siding Spring) by Mars in 2014, and the ensuing meteor shower[8–11]. Of the many elements that ablate from IDPs, Mg^+ and Mg are most readily detectable in ultraviolet (UV) remote sensing, and were observed in a transient layer after the passage of comet Siding Spring[11]. Here we report on remote sensing observations of Mg^+ over the course of MAVEN's two-year mission that are consistent with a persistent meteoric layer. The other dominant species by mass, Fe and Na, would not be observed in a persistent layer due to their reduced scattering efficiencies in the UV[12].

MAVEN's remote sensing instrument for studying Mars' upper atmosphere is the Imaging Ultraviolet Spectrograph (IUVS)[13].

This instrument observes in the far and middle UV (110–190 nm and 190–340 nm) in separate channels, and measures atmospheric emissions from CO_2, its dissociation and ionization products as well as atomic and molecular species such as O and N_2 (refs 14,15). The instrument uses a scan mirror to construct vertical profiles of emergent radiation from the atmosphere at the limb. We use observations from the periapse segment of each orbit, where IUVS produces limb scans over the altitude range 75–250 km. During each orbit, IUVS takes up to 12 limb scans in a ~ 22 min observation period spanning $\sim 45°$ around the planet. MAVEN's elliptical orbit precesses about Mars on timescales of months to provide complete coverage of the planet. Data processing techniques are outlined in detail in previous MAVEN/IUVS papers[11,14–17] and all data used herein are available on the NASA Planetary Data System.

Detection and variability of Mg^+

Emission from Mg^+ was reliably detected in every periapse limb scan obtained over one Mars year (two Earth years; Figs 1–3) whenever the Mg^+ layer was appropriately illuminated and the instrument orientation did not introduce excessive scattered solar continuum (for these purposes, stray light). The Mg^+ emission feature, centred on 280 nm, is due to resonant scattering of solar UV photons rather than direct excitation during ablation. Mg^+ brightnesses were extracted from a model spectrum fit (Fig. 1a,b), using line positions and atomic constants of known emitters in this spectral region plus a stray light solar spectrum[15,16,18].

The Mg^+ emission brightness was converted to local ion density through an Abel transform, common in the study of optically thin airglow emissions[19] (see Supplementary Information). The Mg^+ layer has a mean peak concentration of $\sim 250\,cm^{-3}$ and is typically found near an altitude of 90 km (Fig. 2). Reported altitudes

[1]Laboratory for Atmospheric and Space Physics (LASP), University of Colorado, 80303, USA. [2]School of Chemistry, University of Leeds, Leeds LS2 9JT, UK. [3]Computational Physics, Inc., Springfield, Virginia 22151, USA. [4]Lunar and Planetary Laboratory, University of Arizona, Tucson, Arizona 85721, USA. [5]Center for Space Physics, Boston University, Boston, Massachusetts 02215, USA. [6]Laboratoire de Physique Atmosphérique et Planétaire, Space sciences, Technologies and Astrophysics Research (STAR), University of Liège, B-4000 Liège, Belgium. [7]LATMOS/IPSL, Guyancourt 78280, France.
*e-mail: matteo.crismani@colorado.edu
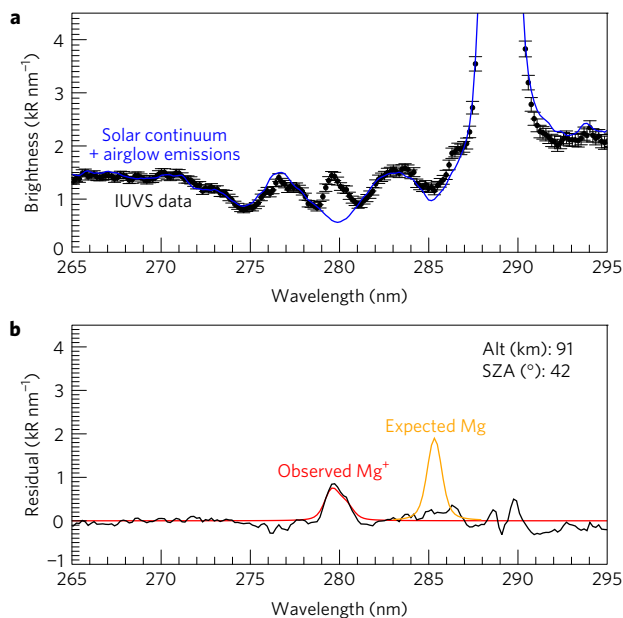
Figure 1 | Spectral identification of Mg⁺. This representative scan was taken near noon (10–15 h local time) in the northern hemisphere (50°–70° N) on 22 April 2016 (orbit 3040). **a**, The spectrum is slit averaged and 1σ error bars are propagated from the Poisson noise of the data. The data are shown as black circles, with known airglow emissions (see text) fitted in blue. **b**, The residual (black line) from **a**, with an emission near 280 nm consistent with Mg⁺ (red) whose brightness is 1.81 ± 0.13 kR. Atomic Mg has an emission feature at 285 nm whose predicted brightness (orange) is not detected (see Fig. 2).

Figure 2 | Altitude profile of Mg⁺ compared with model predictions. IUVS-derived Mg⁺ altitude profiles, averaged from orbit 3040 (the same data shown in Fig. 1), compared with the baseline CABMOD prediction (see Supplementary Information for model details). The predicted brightness is derived from the model density (Fig. 2) using the atomic Mg scattering efficiency[2], indicating (Fig. 1b) that Mg is not detected despite large predicted concentrations.

carry a 2.5 km uncertainty consistent with slit averaging in 5 km bins[16]. Figure 3 shows the derived densities in a fixed altitude range over the course of the mission. Brightness measurements carry Poisson random uncertainties propagated through a multiple linear regression technique and Abel transform. In addition, the brightnesses are subject to 30% systematic uncertainty in absolute calibration (not shown in figure error sizes)[14]. The random and systematic uncertainties propagate linearly into densities and other derived quantities.

Observations of Mg⁺ density demonstrate real variability (Fig. 3) beyond the random uncertainties. First, the lower atmosphere of Mars warms and cools seasonally and in response to dust storms, moving the ablation layer up and down relative to the fixed altitude range used here[20]. Second, the Mg⁺ density decreases by up to a factor of ∼5 towards the dawn and dusk terminators. This effect is most pronounced near the equator and less noticeable near the poles where the diurnal cycle decreases in intensity.

Challenges to existing models

Emission from atomic Mg has been reliably detected (Fig. 1b) only during the exceptionally intense meteor shower of comet Siding Spring[11]. Scaling Mg⁺ by the ratio of the Mg and Mg⁺ scattering efficiencies at our most marginal detection, we find that IUVS would have detected atomic Mg at concentrations greater than 130 cm⁻³. This value falls well below the concentration predicted on the basis of our existing understanding of ablation and atmospheric chemistry (Fig. 2).

The apparent absence of neutral Mg therefore poses a significant challenge to our understanding of the chemical reactions that create and connect Mg and Mg⁺. Laboratory studies validated by terrestrial observations[6] have been incorporated in the Chemical Ablation Model (CABMOD)[21,22], which describes the ablation physics and chemistry, and is coupled to a one-dimensional (1D)

atmospheric model that tracks subsequent atmospheric chemistry (see the Supplementary Information for further details). When adapted for conditions at Mars, CABMOD predicts that Mg atoms would be injected directly during ablation and should build a neutral Mg layer below 100 km. Mg⁺ would then be produced through charge exchange with ambient O_2^+ (ref. 22). Atomic Mg would also undergo a series of reactions to create a steady-state population of $MgCO_3$. Together these reactions are expected to yield a Mg/Mg⁺ ratio of ∼4 at 90 km, contrary to the observed upper limit of ∼0.5. Furthermore, at 90 km Mg⁺ should have a lifetime comparable to a Mars day[21] and should therefore exhibit negligible diurnal variation.

Alternative chemical pathways were investigated to explore the relationship between Mg and Mg⁺. In particular, if the dissociative recombination of $MgCO_3^+$ with electrons yields MgO rather than Mg, then the Mg layer would remain below the IUVS detection limit. (Both the baseline and alternative 1D model results are described more fully in the Supplementary Information.) Additional laboratory studies are needed to accurately determine the branching ratio, and whether other unknown chemistry plays a role. Ongoing efforts to examine the evolution of metallic species following the Siding Spring encounter will appear in a subsequent publication; this period provides the only observed ratios of Mg and Mg⁺, and may further constrain this chemistry. None of the alternative chemical reactions we explored provide an explanation for the strong diurnal variation in Mg⁺.

Constraining the interplanetary dust flux at Mars

The IUVS measurements can be used to provide the first remote sensing estimate of IDP flux at a planet other than Earth. At Earth, the observed metal layer is supplied from the main IDP sources, Jupiter family comets, asteroids, and long-period comets (Halley type and Oort cloud), with particle mass ranging from 10^{-4} and 10^{-7} g, and a global input of 29–57 tonnes d⁻¹ (ref. 23). We do not expect Mars' metal layer to be sourced from a different population, and these observations directly constrain the largest IDP population by mass (excluding surface impactors), making a direct measurement essential for an accurate estimate.
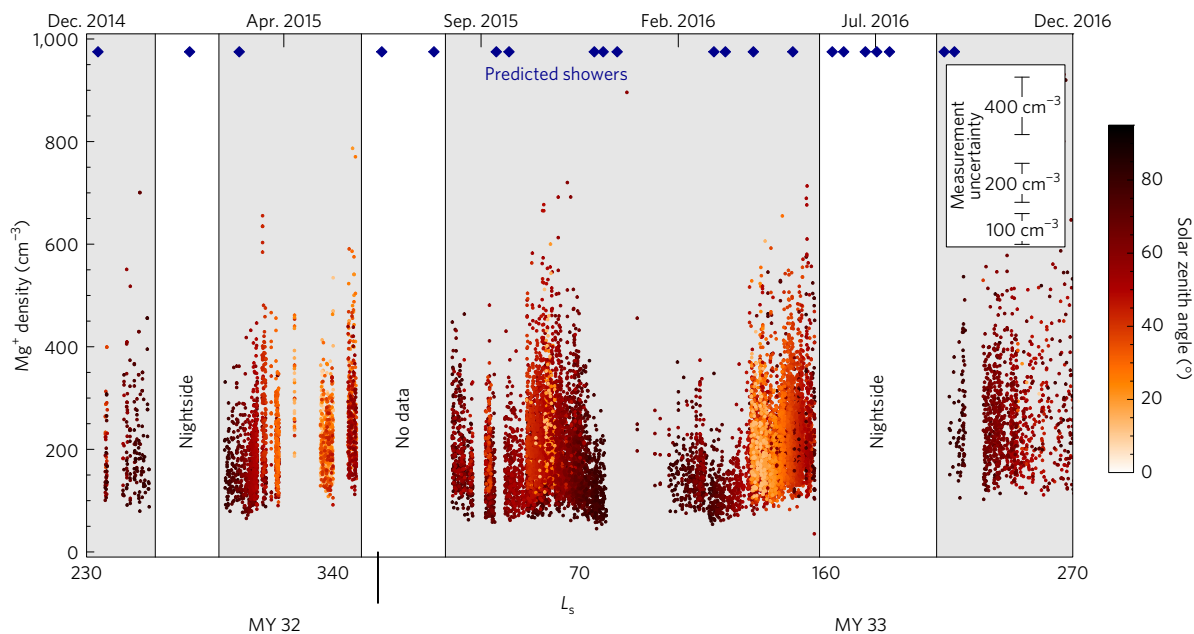
Figure 3 | One Mars year of observations of Mg⁺. Mg^+ concentrations between 90 and 100 km over the course of approximately two Earth years. The timeline omits the comet Siding Spring meteor shower of 19 October 2014, as the peak density of $\sim 10^5$ is off-scale. Average measurement uncertainties are given for three densities in the legend. Observations taken at high solar zenith angle (darker colours, $>70°$) demonstrate marked reduction in Mg^+, consistent with decreases toward the dawn and dusk terminators, especially near the equator. As observations sample a range of latitudes, these observations represent a variety of local time and latitude coverage. Blue diamonds indicate predicted meteor showers (see Supplementary Table 2).

Mars' global dust input was estimated by comparing a Mars zodiacal dust-cloud-derived model[24] to representative profiles with local times near noon and where the peak and underside of the layer were clearly detectable. In the baseline chemical model[21], which neglects the absence of observed Mg, we find a global dust input rate of ~ 2 tonnes sol^{-1}; in the alternative model this value is ~ 3 tonnes sol^{-1} (see the Supplementary Information for details). Note that uncertainties in the $MgCO_3^+$ chemistry render the 2 tonnes sol^{-1} a lower limit, as alternative reactions to reduce the abundance of Mg also reduce the efficiency for creating Mg^+. The instrument's systematic and observational uncertainties are small in comparison with this range in estimates, and therefore are omitted from this result. Comparing the dust environment at Mars with Earth, and accounting for their difference in surface area, we find the fluence at Mars of 2–3 tonnes sol^{-1} is at the lower end of the measurements scaled from Earth[3], 1.4–14 tonnes d^{-1}.

As at Earth, these Mars fluences can be compared to spaceborne dust detectors. The MAVEN Langmuir Probe and Waves instrument measured high-altitude dust particles between 10^{-11}–10^{-7} g and determined a fluence of these particles to be between 85 kg sol^{-1} and 8.5 tonnes sol^{-1} (ref. 25). Their extrapolation to the total input is necessarily imprecise due to the small masses sampled, which is not representative of the mass of IDPs that ablate and inject metals into the atmosphere. The Neutral Gas and Ion Mass Spectrometer (NGIMS) on MAVEN can also sample ablated metals[26], although the region sampled lies several scale heights above the main deposition layer such that global fluence may not be possible to estimate.

Mars is likely to encounter regular meteor showers, analogous to Earth; however, we have been unable to detect any showers other than comet Siding Spring[11], which produced Mg^+ concentrations at 120 km between 5×10^3 and 3×10^4 cm^{-3}. Of the 24 predicted Mars meteor showers since MAVEN's arrival at Mars, IUVS can constrain 11 of these events (Supplementary Table 2) when it was observing in daylight and taking data. The Mg^+ profiles at these times show no correlated increases ≥ 500 cm^{-3} (twice the mean), constraining the fluence of these showers to levels lower than the nominal global input of 3 tonnes sol^{-1}. The two-year timeline of meteoric metal

layer observations reported here then demonstrate that the observed meteor showers do not significantly perturb metal ion abundances. This result is similar to the Earth, where showers have not been conclusively shown to increase its metallic ion content[27].

The observation timeline also argues strongly against a meteoric cause for transient ionospheric layers (the 'M3 layer') detected in radio occultation measurements[28]. The M3 layer was detected in 1–10% of observations, with electron concentrations of 10^4 cm^{-3}. Although a meteoric origin was proposed, the nature of these electron concentrations is ambiguous because the M3 layer may be due to either an enhancement of meteoric (for example, Mg^+, the dominant ion from ablation) or ambient (O_2^+, CO_2^+ and so on) ions. IUVS observations are performed in a similar geometry to radio occultations, and occur every ~ 4.5 h. Therefore, if the source of the M3 layer was metallic ions in concentrations approaching 10^4 cm^{-3}, the layer would be readily observed in 130–1,300 profiles (Fig. 3), whereas IUVS has not detected any Mg^+ densities larger than 10^3 cm^{-3} at any altitude outside of the comet Siding Spring epoch. Another origin, such as enhanced solar energetic particle precipitation or X-ray flux, may be responsible for the transient M3 layer.

Methods

Methods, including statements of data availability and any associated accession codes and references, are available in the online version of this paper.

References

1. Istomin, V. Ions of extraterrestrial origin in the Earth atmosphere. *Planet. Space Sci.* **11,** 173–174 (1963).
2. Anderson, J. & Barth, C. Rocket investigation of the Mg I and Mg II dayglow. *J. Geophys. Res.* **76,** 3723–3732 (1971).
3. Plane, J. Cosmic dust in the earth's atmosphere. *Chem. Soc. Rev.* **41,** 6507–6518 (2012).
4. Vondrak, T. *et al.* A chemical model of meteoric ablation. *Atmos. Chem. Phys.* **8,** 7015–7031 (2008).

5. Plane, J., Feng, W. & Dawkins, E. The mesosphere and metals: chemistry and changes. *Chem. Rev.* **115**, 4497–4541 (2015).
6. Nachbar, M., Duft, D. & Mangan, T. Laboratory measurements of heterogeneous CO_2 ice nucleation on nanoparticles under conditions relevant to the Martian mesosphere. *J. Geophys. Res.* **121**, 753–769 (2016).
7. Jakosky, B. *et al*. The Mars atmosphere and volatile evolution (MAVEN) mission. *Space Sci. Rev.* **195**, 3–48 (2015).
8. Benna, M. *et al*. Metallic ions in the upper atmosphere of Mars from the passage of comet C/2013 A1 (Siding Spring). *Geophys. Res. Lett.* **42**, 4670–4675 (2015).
9. Gurnett, D. *et al*. An ionized layer in the upper atmosphere of Mars caused by dust impacts from comet Siding Spring. *Geophys. Res. Lett.* **42**, 4745–4751 (2015).
10. Restano, M. *et al*. Effects of the passage of Comet C/2013 A1 (Siding Spring) observed by the Shallow Radar (SHARAD) on Mars Reconnaissance Orbiter. *Geophys. Res. Lett.* **42**, 4663–4669 (2015).
11. Schneider, N. *et al*. MAVEN IUVS observations of the aftermath of the Comet Siding Spring meteor shower on Mars. *Geophys. Res. Lett.* **42**, 4755–4761 (2015).
12. Kramida, A., Ralchenko, Y. & Reader, J. NIST ASD Team *NIST Atomic Spectra Database* (*ver. 5.3*) (Online, 2015).
13. McClintock, W. *et al*. The imaging ultraviolet spectrograph (IUVS) for the MAVEN mission. *Space Sci. Rev.* **195**, 75–124 (2015).
14. Evans, J. *et al*. Retrieval of CO_2 and N_2 in the Martian thermosphere using dayglow observations by IUVS on MAVEN. *Geophys. Res. Lett.* **42**, 9040–9049 (2015).
15. Stevens, M. *et al*. New observations of molecular nitrogen in the Martian upper atmosphere by IUVS on MAVEN. *Geophys. Res. Lett.* **42**, 9050–9056 (2015).
16. Jain, S. *et al*. The structure and variability of Mars upper atmosphere as seen in MAVEN/IUVS dayglow observations. *Geophys. Res. Lett.* **42**, 9023–9030 (2015).
17. Crismani, M. *et al*. Ultraviolet observations of the hydrogen coma of comet C/2013 A1 (Siding Spring) by MAVEN/IUVS. *Geophys. Res. Lett.* **42**, 8803–8809 (2015).
18. Dymond, K. *et al*. Middle ultraviolet emission from ionized iron. *Geophys. Res. Lett.* **30**, 1003 (2003).
19. Chamberlain, J. & Hunten, D. *Theory of Planetary Atmospheres. An Introduction to their Physics and Chemistry* (Academic, 1987).
20. Jakosky, B. *et al*. Mars' atmospheric history derived from upper-atmosphere measurements of $^{38}Ar/^{36}Ar$. *Science* **355**, 1409–1410 (2017).
21. Whalley, C. & Plane, J. Meteoric ion layers in the Martian atmosphere. *Faraday Discuss.* **147**, 349–368 (2010).
22. Molina-Cuberos, G. *et al*. Meteoric ions in the atmosphere of Mars. *Planet. Space Sci.* **51**, 239–249 (2003).
23. Carrillo-Sánchez, J. *et al*. Sources of cosmic dust in the Earth's atmosphere. *Geophys. Res. Lett.* **43**, 11979–11986 (2016).
24. Nesvorný, D. *et al*. Cometary origin of the zodiacal cloud and carbonaceous micrometeorites. Implications for hot debris disks. *Astrophys. J.* **713**, 816 (2010).
25. Andersson, L. *et al*. Dust observations at orbital altitudes surrounding Mars. *Science* **350**, 6261 (2015).
26. Grebowsky, J. *et al*. Unique, non-earthlike, meteoritic ion behavior in the upper atmosphere of Mars. *Geophys. Res. Lett.* **44**, http://dx.doi.org/10.1002/2017GL072635 (2017).
27. Grebowsky, J. & Aikin, A. *In Situ Measurements of Meteoric Ions* (Cambridge Univ. Press, 2002).
28. Pätzold, M. *et al*. A sporadic third layer in the ionosphere of Mars. *Science* **310**, 837–839 (2005).

Author contributions

M.M.J.C., S.K.J., J.S.E., J.I.D. and M.S.C. improved the data processing to create these data products. M.M.J.C., N.M.S. and J.M.C.P. developed the interpretation of this data. J.M.C.P. and J.D.C.-S. created the model used herein. All authors contributed to the development of the instrument pipeline and/or data acquisition as well as interpretation and presentation of these results.

Additional information

Supplementary information is available in the online version of the paper. Reprints and permissions information is available online at www.nature.com/reprints. Publisher's note: Springer Nature remains neutral with regard to jurisdictional claims in published maps and institutional affiliations. Correspondence and requests for materials should be addressed to M.M.J.C.

Competing financial interests

The authors declare no competing financial interests.

Methods

Mg^+ density retrieval. To determine the density at the tangent point, we used an Abel transform method[18], considering the emission to be optically thin and a spherically symmetric observing geometry. Using the standard relationship for the scattering cross-section, related to the oscillator strength and Doppler width[29], we find the Mg^+ doublet (at 140 K) cross-section is 8.9 and 4.4×10^{-12} cm^2. Therefore, we do not expect self-scattering to become important until densities at the tangent point approach 10^4 cm^{-3}, and the path length is reduced to 100 km. As the retrieved densities are never larger than 10^3 cm^{-3}, we consider this emission optically thin; thus, the Abel transform is a robust approximation to the density at the tangent point.

The g-factors for the Mg^+ lines at 279.5528 and 280.2705 nm used herein are 10.05×10^{-2} s^{-1} and 4.64×10^{-2} s^{-1} respectively. Two groups have calculated these g-factors: recently[18] found to be 8.4×10^{-2} s^{-1} and 3.9×10^{-2} s^{-1} (previously[2] found to be 9.1×10^{-2} s^{-1} and 3.7×10^{-2} s^{-1}). Although the newer calculation[18] cites their use of a higher-resolution solar spectrum[30], the spectrum found therein is actually not higher resolution, and a personally communicated spectrum from ref. 30, which we used, may be instead what they were referencing. In this spectrum, the flux at 1 AU is 2.5 and 2.2×10^{12} for 279.6 and 280.3 nm respectively. For the Mg line, we use the g-factor used in ref. 2.

1D model details. The 1D model used for this study has been described in detail by Whalley and Plane[21]. The eddy diffusion coefficient (K_{zz}) profile in Supplementary Fig. 1 is taken from ref. 31: the value of 2×10^6 cm^2 s^{-1} below 65 km was estimated from Phobos 2 solar occultation measurements of dust, ozone and clouds at low latitudes. The larger values ($>10^7$ cm^2 s^{-1}) above 100 km are consistent with the K_{zz} required to model measurements made by the Viking 1 and 2 spacecraft[32] and the values that have been used in other 1D models[33,34]. The molecular diffusion coefficient profiles of Mg and Mg^+ are also illustrated in Supplementary Fig. 1, showing that the turbopause height is around 120 km—consistent with measurements made by the Neutral Gas Ion Mass Spectrometer instrument on MAVEN[8,25] during deep-dip orbits down to 130 km.

The off-line sources of the vertical profiles of the minor trace species O_3, O, O_2, H, CO, O_2^+, and electrons, for daytime low-latitude conditions, are described in ref. 21. Supplementary Fig. 2 compares the production rates of Mg^+ from photo-ionization and charge transfer with the major ambient O_2^+ ion, showing that charge transfer dominates between 90 and 190 km.

Supplementary Table 1 contains rate coefficients for the reaction scheme used in the 1D model. Most of these rate coefficients have now been measured over the temperature and pressure ranges needed to extrapolate with reasonable confidence to the conditions on Mars (see the footnotes to the Supplementary Table). The rate coefficient for the reaction

$$MgO^+ + CO_2(+CO_2) \rightarrow MgCO_3^+$$
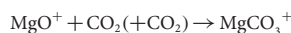
was calculated using electronic structure theory to determine the reaction enthalpy (149 kJ mol^{-1} at the cbs-qb3 level of theory) and molecular parameters, and then applying Rice–Ramsperger–Kassel–Marcus theory[35]. Dissociative recombination of the $MgCO_3^+$ ion with an electron is assumed to have two reaction channels:

$$MgCO_3^+ + e^- \rightarrow MgO + CO_2 \quad \alpha$$

$$\rightarrow Mg + O + CO_2 \quad (1 - \alpha)$$
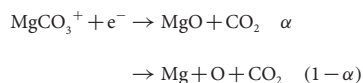
where α is the branching ratio.

Meteoric ablation is assumed to be the source of Mg species, and the Mg ablation profile peaking at ~80 km in the 1D model—adapted for Mars with representative meteoroid mass and velocity distributions (see ref. 21 for details)—was optimized to give agreement of the modelled and IUVS-measured peak of the Mg^+ profile around 95 km.

The model was then run until steady-state conditions were reached (typically 20 days). The objective of the modelling was to explain the observed Mg^+ profile, and the lack of a detectable Mg signal above the IUVS threshold of 130 cm^{-3} at 90 km. If meteoric ablation injects the magnesium mainly as Mg atoms, then the lack of a pronounced Mg layer cannot be explained in terms of the known chemistry of Mg. This is because the very unreactive Mg atoms should react with only O_3 or O_2^+ in the Mars atmosphere below 100 km (Supplementary Table 1),

and neither of these reactants has a high concentration[6]. One possibility is that when Mg atoms evaporate during ablation, they are initially travelling at hyperthermal velocities (>5 km s^{-1}) and therefore have more than enough impact energy to react with CO_2 to make $MgO + CO$ (a reaction that is endothermic by 272 kJ mol^{-1}; ref. 36). In the model runs discussed below, it is assumed that ablation produces 90% MgO below 100 km, and 90% of Mg^+ at higher altitudes (which is where the faster-moving meteoroids ablate, leading to a greater probability of ionization[36]).

The model was used to test the effect of varying α on the modelled Mg^+ and Mg layers. The results of setting $\alpha = 0.01$ and 1 are illustrated in Supplementary Figs 3 and 4, respectively. With the small value of α most of the $MgCO_3^+$ dissociates to Mg following electron recombination. The enhanced Mg then produces more Mg^+ below 90 km, so that the underside of the Mg^+ layer is then in very good agreement with the IUVS observations, as is the case for the rest of the layer above 90 km (Supplementary Fig. 3). For this simulation, a Mg ablation flux of 6,900 cm^{-2} s^{-1} is required. Note, however, that the Mg layer now peaks at 490 cm^{-3}, a factor of 3.8 above the IUVS detection threshold.

In contrast when $\alpha = 1$, dissociative recombination produces MgO, which rapidly recombines with CO_2 to make $MgCO_3$, and this in turn reacts with H_2O to form the stable Mg reservoir $Mg(OH)_2$ (ref. 36). As shown in Supplementary Fig. 4, the Mg layer is now reduced to below the IUVS threshold. However, the underside of the Mg^+ layer cuts off more sharply than observed—although that is a less important criterion than the absence of detectable Mg. For this simulation, the Mg ablation flux needs to be increased to 10,900 cm^{-2} s^{-1}.

Extrapolating globally the ablation input of Mg, distinct from unmelted micrometeorites and cosmic spherules, would then be 0.057 tonnes sol^{-1}. Unmelted material can be determined from our understanding of the terrestrial atmosphere, where a recent study of the contributions of cosmic dust from Jupiter family comets, asteroids and long-period comets concluded that overall 1 tonne of Mg ablated from 43 tonnes of dust[22]. Translating this ratio to Mars where the fraction ablating is slightly lower because of the reduced entry velocity of the dust particles[20], 1 tonne of Mg ablates from about 55 tonnes of dust. This implies that the total dust input at Mars is 3.2 tonnes sol^{-1}.

References

29. Risberg, P. The spectrum of singly-ionized magnesium, MG-II. *Arkiv Fysik* **9**, 483–494 (1955).
30. A'Hearn, M. F., Ohlmacher, J. T. & Schleicher, D. G. *A High Resolution Solar Atlas for Fluorescence, Calculations* Technical Report: TR AP83-044 (University of Maryland, 1983).
31. Rosenqvist, J. & Chassefiere, E. A re-examination of the relationship between eddy mixing and O_2 in the Martian middle atmosphere. *J. Geophys. Res.* **100**, 5541–5551 (1995).
32. Izakov, M. N. Martian upper atmosphere structure from the Viking spacecraft experiments. *Icarus* **36**, 189–197 (1978).
33. Pesnell, W. D. & Grebowsky, J. Meteoric magnesium ions in the Martian atmosphere. *J. Geophys. Res.* **105**, 1695–1707 (2000).
34. Rodrigo, R., Garcia-Alvarez, E., Lopez-Gonzalez, M. J. & Lopez-Moreno, J. J. A nonsteady one-dimensional theoretical model of Mars' neutral atmospheric composition between 30 and 200 km. *J. Geophys. Res.* **95**, 14795–14810 (1990).
35. Whalley, C. L., Gomez Martin, J. C., Wright, T. G. & Plane, J. M. C. A kinetic study of Mg^+ and Mg-containing ions reacting with O_3, O_2, N_2, CO_2, N_2O and H_2O: implications for magnesium ion chemistry in the upper atmosphere. *Phys. Chem. Chem. Phys* **13**, 6352–6364 (2011).
36. Plane, J. M. C. & Whalley, C. L. A new model for magnesium chemistry in the upper atmosphere. *J. Phys. Chem. A* **116**, 6240–6252 (2012).